

# Identification of karst sinkholes in a forested karst landscape using airborne laser scanning data and water flow analysis

Jaroslav Hofierka<sup>a,\*</sup>, Michal Gallay<sup>a</sup>, Peter Bandura<sup>b</sup>, Ján Šašák<sup>a</sup>

<sup>a</sup> Institute of Geography, Faculty of Science, Pavol Jozef Šafárik University in Košice, Jesenná 5, 04001 Košice, Slovak Republic

<sup>b</sup> Department of Physical Geography and Geoecology, Faculty of Natural Sciences, Comenius University in Bratislava, 842 15, Slovak Republic

## ARTICLE INFO

### Article history:

Received 26 January 2017

Received in revised form 20 October 2017

Accepted 2 February 2018

Available online 10 February 2018

### Keywords:

Sinkholes

LiDAR

Water flow

DEM

## ABSTRACT

Karst sinkholes (dolines) play an important role in a karst landscape by controlling infiltration of surficial water, air flow or spatial distribution of solar energy. These landforms also present a limiting factor for human activities in agriculture or construction. Therefore, mapping such geomorphological forms is vital for appropriate landscape management and planning. There are several mapping techniques available; however, their applicability can be reduced in densely forested areas with poor accessibility and visibility of the landforms. In such conditions, airborne laser scanning (ALS) provides means for efficient and accurate mapping of both land and landscape canopy surfaces. Taking the benefits of ALS into account, we present an innovative method for identification and evaluation of karst sinkholes based on numerical water flow modelling. The suggested method was compared to traditional techniques for sinkhole mapping which use topographic maps and digital terrain modelling. The approach based on simulation of a rainfall event very closely matched the reference datasets derived by manual inspection of the ALS digital elevation model and field surveys. However, our process-based approach provides advantage of assessing the magnitude how sinkholes influence concentration of overland water flow during extreme rainfall events. This was performed by calculating the volume of water accumulated in sinkholes during the simulated rainfall. In this way, the influence of particular sinkholes on underground geomorphological systems can be assessed. The method was demonstrated in a case study of Slovak Karst in the West Carpathians where extreme rainfalls or snow-thaw events occur annually. We identified three spatially contiguous groups of sinkholes with a different effect on overland flow concentration. These results are discussed in relation to the known underground hydrological systems.

© 2018 Elsevier B.V. All rights reserved.

## 1. Introduction

Sinkholes or dolines are closed land surface depressions with internal drainage typically formed in karst environments (Ford and Williams, 2007). They play a vital role in local control of spatial distribution of water and air flows. Water and air converge in a sinkhole and by this means the morphology of the sinkhole affects water flow movement, soil erosion and accumulation, soil moisture and depth, or air temperature and humidity (Antonic et al., 2001). Presence of sinkholes poses a risk to agriculture, construction, and other human activities by collapsing or sagging of bedrock, suffosion, or flooding (Gutiérrez et al., 2014). Sinkholes preserve biodiversity by being important refugia for specific plant species (Bátori et al., 2014). Delineation and inventory of karst features are important because of the susceptibility of karst landscape to groundwater contamination and the unique problems associated with construction of buildings and roads in karst areas. Many countries,

for this reason, embarked on creating a national geodatabase of sinkholes (e.g., Gao et al., 2002; Farrant and Cooper, 2008; PaDCNP, 2016).

Traditionally, sinkholes were mapped in the field with the aid of topographic maps or by visual inspection of aerial imagery (e.g., Panno and Weibel, 1996; Zboray and Bárány Kevei, 2004; Alexander et al., 2013; Luman and Panno, 2013), oblique radar intensity images (Jakál et al., 1992), or multispectral satellite imagery (Siart et al., 2009). Such an approach has been less applicable in forested karst where sinkholes are obscured by dense tree canopy. A poor accessibility may also limit methods such as ground surveying with tacheometry or global navigation satellite systems (GNSS). These are also more suitable for smaller areas than for regional mapping (Barabas et al., 2010). Much higher level of detail in mapping sinkholes can be achieved with close-range photogrammetry from unmanned airborne systems and with terrestrial laser scanning although these techniques are also more relevant for small scale studies such as Tilly et al. (2016).

The limitations of forest canopy in regional scale studies can be overcome by active remote sensing methods from airborne platforms such as synthetic aperture radar interferometry (InSAR) or laser scanning also known as LiDAR (Wulder and Franklin, 2012). Airborne

\* Corresponding author.

E-mail address: [jaroslav.hofierka@upjs.sk](mailto:jaroslav.hofierka@upjs.sk) (J. Hofierka).

laser scanning (ALS) is capable of a much more detailed and more accurate measuring of land surface elevations than InSAR, but ALS is less competitive in dense tropical humid rainforests. The InSAR technique uses microwave electromagnetic waves which penetrate through such forest to the ground, however, compromising this advantage by a lower spatial resolution in order of several metres in comparison with ALS (e.g., [Gutiérrez et al., 2011](#); [de Carvalho Júnior et al., 2014](#); [Schlund et al., 2015](#)). With regard to the forest canopy closure, ALS is especially useful in mid-latitudes for mapping land surface under scrubs or forests. The laser scanner detects portions of the reflected laser energy through the canopy where other mapping techniques are ineffective or not applicable. ALS has been preferred and it has been extensively used for detailed mapping of gullies ([James et al., 2007](#)), sinkholes ([Seale et al., 2008](#)), hummocks ([Li et al., 2011](#)), or landslides ([Van den Eeckhaut et al., 2012](#)). Applications of ALS in dense tropical forest were also successful in detection of cenotes as cave entrances ([Weishampel et al., 2011](#)).

Advances in geomorphometry and implementation of various interpolation techniques in a geographic information system (GIS) ([Neteler and Mitasova, 2008](#); [Hengl and Reuter, 2008](#); [Bishop et al., 2012](#)) enabled mapping karst morphology by the means of digital elevation models (DEMs) which represent land (ground) surface. Before the widespread use and distribution of ALS-derived elevation data, the photogrammetrically derived contours used to be the most popular source of elevation data for digital geomorphometric analyses. Contour-based DEMs were used for regional studies of karst morphology ([Antonic et al., 2001](#); [Angel et al., 2004](#); [Pardo-Igúzquiza et al., 2013](#)). Karst sinkholes of greater extent were mapped using lower resolution DEM resources such as SRTM or ASTER ([de Carvalho Júnior et al., 2014](#)) which were combined with satellite imagery ([Siart et al., 2009](#)).

Recently available elevation data from the TerraSAR-X and TanDEM-X mission has brought new potential in mapping relatively small geomorphological features such as sinkholes using from space-borne InSAR-based DEMs ([Pipaud et al., 2015](#)). However, all these satellite-based DEM resources are considered as digital surface models (DSMs), because they include the height of vegetation and buildings. Thus their applicability to sinkhole mapping under a dense forest canopy is rather limited.

Four main groups of methods can be identified according to the review of published research on karst depression mapping with DEMs or vectorised elevation contours. The first group of studies used visual inspection of hill-shaded DEMs ([Luman and Panno, 2013](#); [Shadem et al., 2013](#); [Alexander et al., 2013](#)). Second approach utilized the outermost closed contour as the outline of a sinkhole ([Zboray and Bárány Kevei, 2004](#); [Angel et al., 2004](#); [Telbisz and Mőga, 2005](#); [Telbisz et al., 2006](#); [Seale et al., 2008](#); [Bauer, 2015](#); [Telbisz et al., 2016](#); [Wall et al., 2017](#)). Such an approach coupled with hierarchical classification of sinkholes based on graph theory was recently implemented by [Wu et al. \(2016\)](#). The third group of studies comprises methods based on sink-filling of DEMs. Essentially, sink-filling involves various flow routing algorithms (e.g., [Jenson and Domingue, 1988](#); [MacMillan et al., 2003](#)) which identify depression points in the DEM surface (also termed sinks or pits). The depressions are filled given the depth threshold and the sink-filled DEM is subtracted from the original DEM in a map algebra operation. Grid layer containing areas of depressions originates as a result of the procedure ([Antonic et al., 2001](#); [Doctor and Young, 2013](#); [de Carvalho Júnior et al., 2014](#); [Telbisz et al., 2016](#); [Wall et al., 2017](#)). Other auxiliary data (e.g., geologic maps, road network, orthoimagery), expert knowledge, or field survey are needed with this method to differentiate between real land surface depressions and DEM surface artefacts

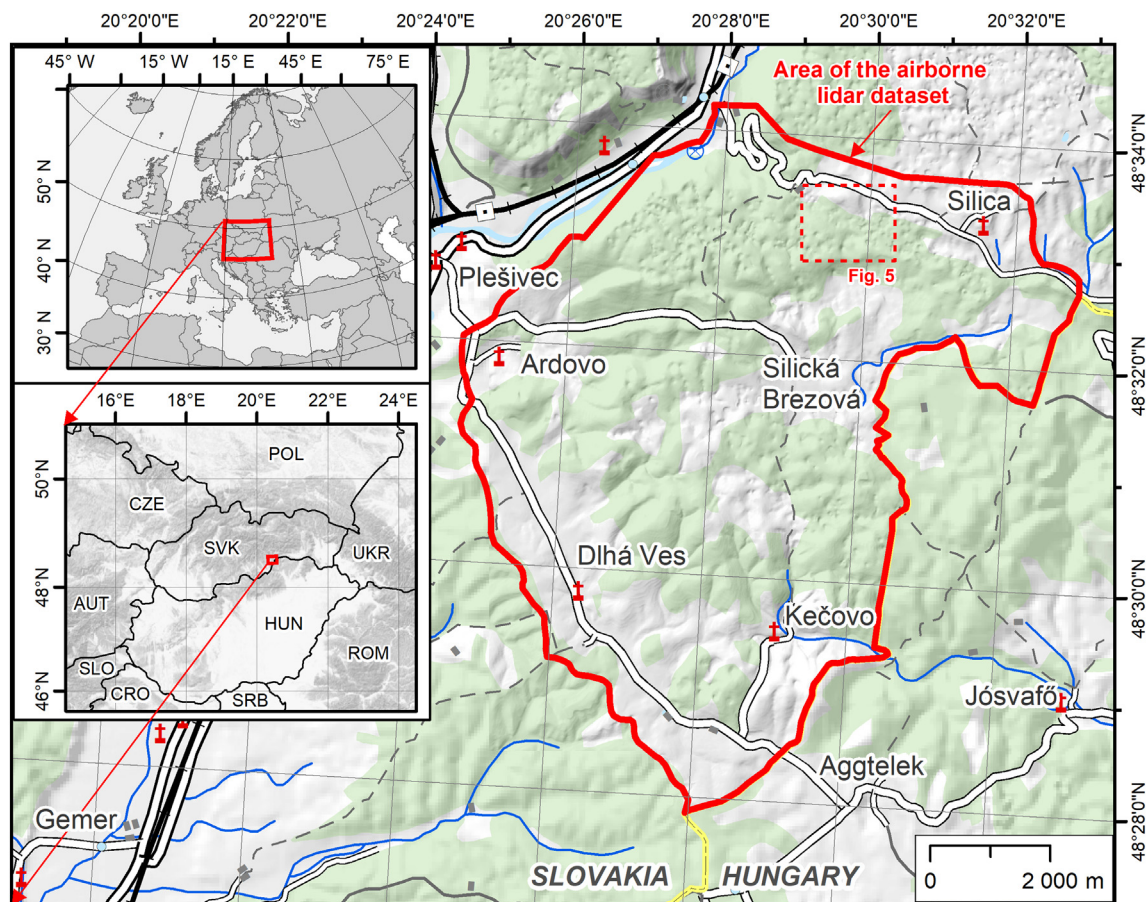


**Fig. 1.** Location of the karst area mapped with the airborne laser scanning. The green (darker) areas indicate forested land. The red dashed line outlines the extent of the area in [Fig. 5](#).



(e.g., Wall et al., 2015). Lastly, the fourth group of methods involves some kind of a moving window operator (i.e. a kernel window) to evaluate the relative position of each DEM cell with respect to neighbourhood surrounding the cell. In this way, Weishampel et al. (2011) or Doctor and Young (2013) used topographic position index which parameterizes the difference between elevation at inspected DEM cell and the mean elevation of its neighbourhood. Obu and Podobnikar (2013) used a combined approach of flow routing for locating depression points and a focal function in a moving window for defining the outline of the depression. Their approach has been used to define sinkholes under forest in Kobal et al. (2015).

The review suggests that sinkholes, as the target forms of DEM analysis, have not been subject to approach based on modelling a natural process such as analysis of overland flow during heavy rainfalls. Nor the influence of sinkholes on this process has been evaluated. Recent developments of more robust simulation techniques in terms of applying the Monte Carlo method (Mitas and Mitasova, 1998; Hofierka and Knutová, 2015; Jeziorska et al., 2016) for water flow routing provided new tools that can be effectively used for identification of land surface depressions which accumulate overland water flow. In overland water flow modelling, the purpose is to remove all artefactual

topographic depressions while real ones remain preserved. Standard procedures in practice, however, assume that all topographic depressions are artefacts thus these are all removed from the DEM (Lindsay and Creed, 2006; Wechsler, 2007). This assumption is frequently untrue especially in karst topographies, although artificial depressions can be present in the DEM.

The aim of this paper is to present an original methodology for mapping karst sinkholes under the dense forest canopy using the ALS data and numerical water flow modelling. The objective is to identify the sinkholes using various methods and to differentiate the sinkholes according to their ability to concentrate water flow. We show that the appropriate ALS data preparation can improve the quality of mapping specific karst landforms in the forest by comparing their identification based on topographic maps derived photogrammetrically as oppose to other approaches based on geomorphometric analysis of ALS DEMs representing the land surface.

## 2. Study area

The area of interest (67 km<sup>2</sup>) is a part of the National Park of Slovak Karst near the state border of Slovakia with Hungary, Central Europe

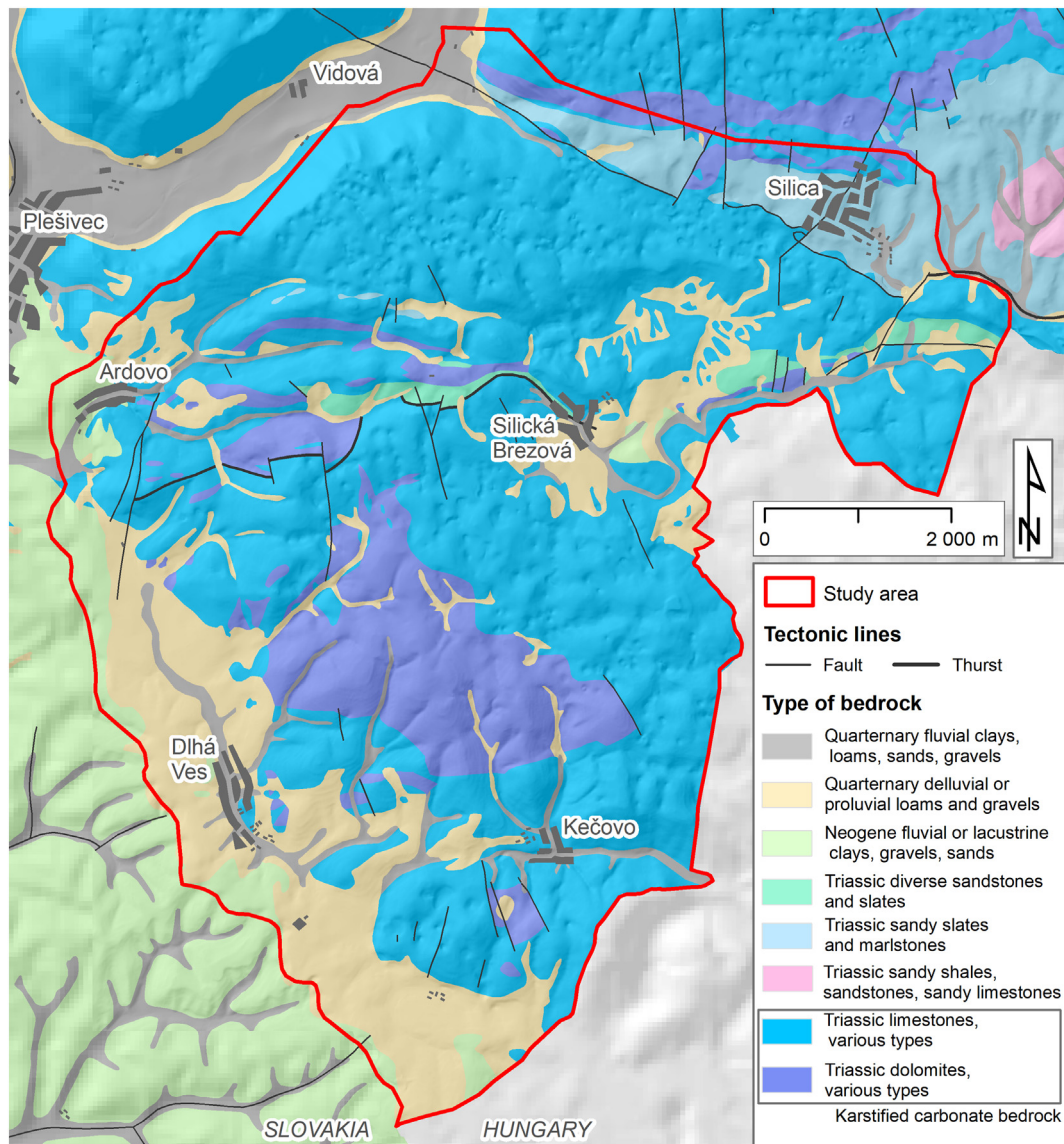


**Fig. 2.** Bedrock geology in the study area after Mello (1996) with the hill-shaded ALS DEM in the background. The karstified carbonate bedrock comprises the last two rock formations in the legend.

**Table 1**

Parameters of the ALS mission flown with a Leica ALS70-CM lidar system.

Parameter	Value
Flight height above ground	405–764 m
Flight altitude above mean sea level	1031 m
Total number of points	1990 million
Total area	67 km <sup>2</sup>
Average density of returns (all/ground)	29 points m <sup>-2</sup> /21 points m <sup>-2</sup>
Ground returns density (all/under forest)	5 points m <sup>-2</sup> /0.5 points m <sup>-2</sup>
Absolute overall accuracy in open areas	0.1 m @ 1 $\sigma$

(Fig. 1). Slovak Karst is formed by several karst plateaux situated at altitudes of 400–700 m above mean sea level with decreasing elevation from the north to the south. The plateaux are separated by 100–300 m deep canyons and valleys. The study area comprises the south-western part of the Silická planina Plateau (Jakál, 1975). The land is covered by deciduous forests (59%) where oak and hornbeam are the most common species (Balogh and Barabas, 2016). The rest of the study area comprises grassland (22%), shrubs (5%), and arable land (9%). This region is precious for the specifics of a mid-latitude karst landscape (Rozložník, 1998) for which several landform features are typical, such as dolines, blind valleys, sinkholes, and karrens. These features are difficult to be mapped in a forested land or in shrubs by traditional surveying or photogrammetry though airborne lidar mapping is highly applicable. However, no national lidar database exists in Slovakia up to date; therefore, the selected karst area was flown within our custom laser scanning mission in July 2014.

Slovak Karst is adjacent to the Aggtelek Karst in Hungary. Aggtelek and the south part of Silická planina Plateau in Slovakia are tectonically separated from the north part of Slovak Karst by the fault zone leading from the town of Plešivec through Silická Brezová towards the Turnianska kotlina Basin in the eastern part of Slovak Karst (Gaál, 2008). From the morphological point of view, this lineament forms a border between the Slovenské rudohorie Subregion and the South-Eastern Marginal Subregion of the Western Carpathians (Minár et al., 2011). Tectonic framework was generated by south to southeast oriented pressures which caused stress, and the compression was realised in the range of directions of north-south to northwest-southeast (Gaál, 2008). The landscape evolved on carbonate rocks comprising mainly Triassic limestones and dolomites of the Silica Nappe (Fig. 2). The carbonates formed on Lower Triassic Verfenian shales which outcrop along the west to east oriented zone passing the village of Silica.

The geological and morphological settings of the area are the main reasons why there are only few permanent streams. Most of the surficial water infiltrates underground or generates only temporary streams which flow into abundant ponors under the ground. The area of interest is abundant with many caves (Hochmuth, 2008) indicating that superficial and underground processes strongly interact. Many caves developed as a continuation of ponors which drain the overland water flow under the ground. In the recent history, several rainfall events caused major flooding in the Domica cave system. The flooding was induced by inappropriate agricultural practice on the cultivated land (Bella, 2001; Gaálová et al., 2014; Kováč et al., 2014). Hochmuth and Gessert (2016) also recorded the effect of flash floods in the Domica

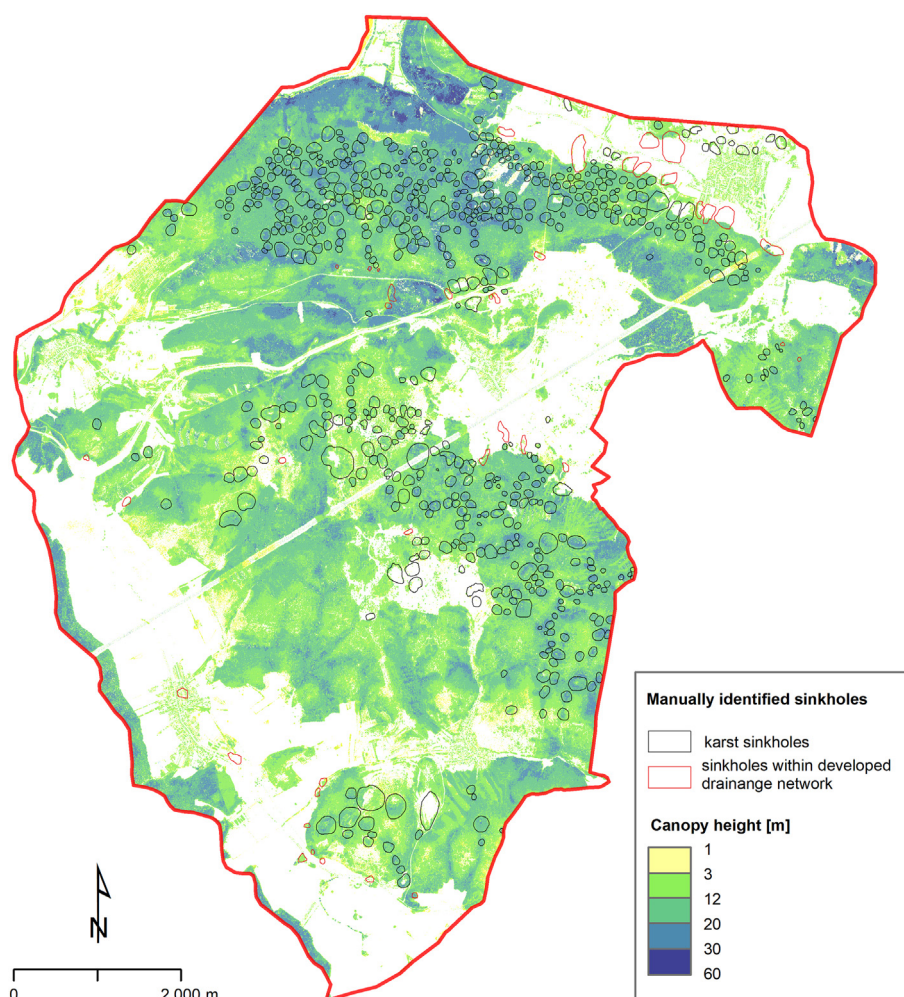


**Fig. 3.** Forest canopy height model derived from the ALS data with overlaid outlines of sinkholes identified from the ALS data.



cave in February 2016. The cave was subject to terrestrial laser scanning and 3D modelling of the cave surface (Gallay et al., 2015, 2016) which provided means for better understanding of the cave hydrological system. The cross-border cave system Domica-Baradla is a listed UNESCO World heritage site and a part of it is a show cave visited by tourists.

### 3. Methods and data

#### 3.1. Airborne laser scanning and digital terrain modelling

The ALS dataset originated during a mission flown in July 2014 by Photomap s.r.o., Košice over the area delineated in Fig. 2. Table 1 summarizes the key mission parameters. The relatively high density of ground returns even under forest (0.5 point per  $\text{m}^2$ ) was important to capture all kinds of geomorphic features even under dense canopy. The ALS data are supplemented with RGB and near-infrared orthoimagery acquired in April 2014 by airborne photogrammetry (ground sampling distance of 0.2 m). The image data were used to colourize the points.

The ALS data were supplied as geometrically corrected and partially classified point cloud which was georeferenced in the S-JTSK East North coordinate system and the Baltic height datum after adjustment. The cloud was split into data tiles of  $500 \times 500$  m in the LAS 1.2 format for further handling. Processing of the raw ALS data was conducted using the TerraScan proprietary software by TerraSolid on the side of the

data supplier, Photomap s.r.o., Košice. We further processed data using LAStools (Isenburg, 2014) to check and prepare the laser scanning point cloud for generating the grid-based digital surface models and elevation models (Hofierka et al., 2017a). The original lidar data tiles were processed to remove the data noise and classified into four categories: ground, vegetation, buildings, and unclassified. The point data tiles were used to derive seamless grids representing a DEM of land surface (bare ground) and a DSM that includes the land cover surface. The relative height of vegetation above ground (i.e. normalized height, canopy height) depicted in Fig. 3 was calculated by subtracting the DEM from the DSM (Fig. 3).

Firstly, we generated a DEM directly from all ground returns (300 million points) in LAStools but the DEM contained considerable amount of noise including microtopographic features. In this case, the DEM was derived by linear interpolation of point elevations into grid nodes during the TIN-to-grid conversion. This is especially visible in the spatial pattern of parameters derived from the DEM such as slope steepness or curvature that are very sensitive to even subtle local variation of elevations. Therefore, for our purposes, it is more appropriate to model the land surface on a larger scale (lower level of detail) using a smooth interpolation function which generates a smoothly varying DEM surface. For this reason, we opted for the v.surf.rst interpolation module in GRASS GIS (Neteler and Mitasova, 2008; Neteler et al., 2012; GRASS Development Team, 2017) which enables fine tuning of the input parameters (Mitasova

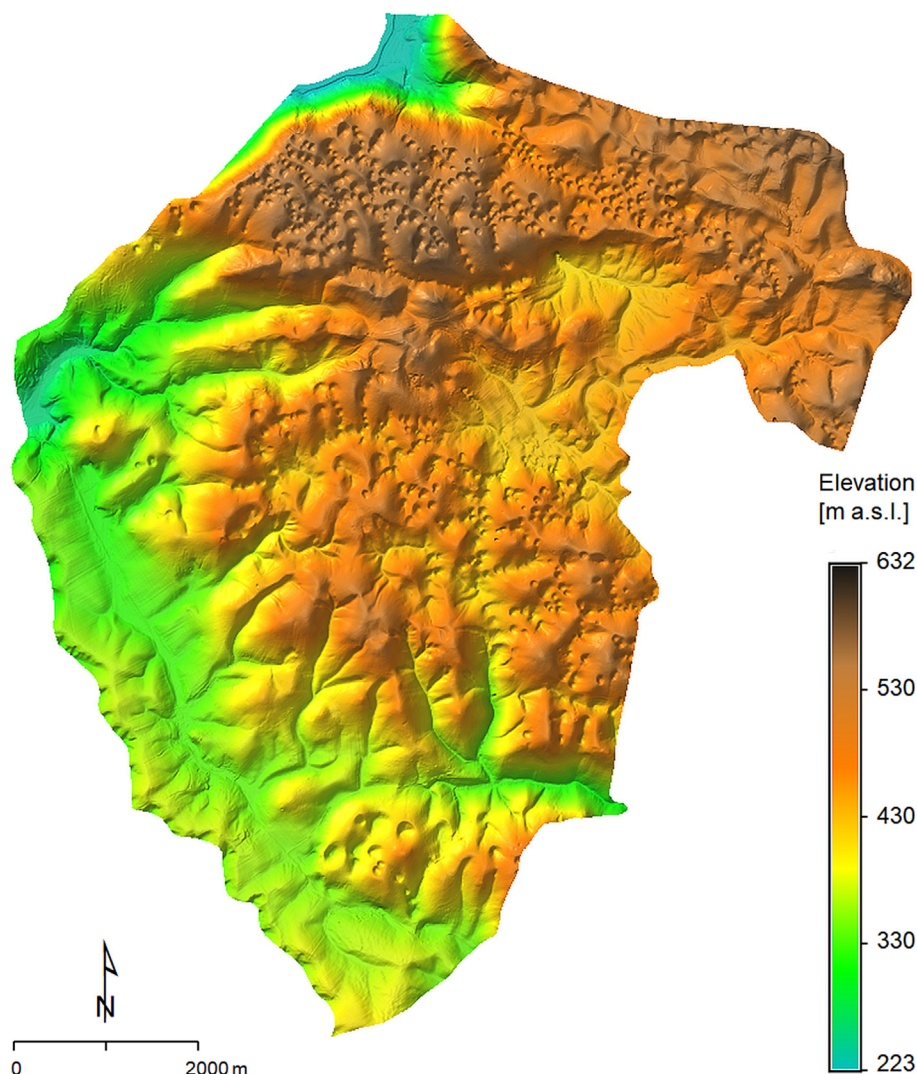


Fig. 4. Hill-shaded DEM derived at 5-m cell size from the reduced ALS data and interpolated by v.surf.rst in GRASS GIS.

et al., 2005; Hofierka et al., 2013). The method uses a regularized spline with tension and smoothing function (Mitáš and Mitášová, 1993) and it is widely used for its flexibility in tuning input parameters. We reduced the original point cloud of ground laser returns to 75 million of points resulting in an average point density of  $1.1 \text{ point m}^{-2}$ . Processing such a massive dataset in current GIS software is not trivial even after the decimation of the points. For example, it would take about 33 h of computing time to process these data at 1 m spatial resolution using the v.surf.rst interpolation module and using a standard desktop computer. Therefore, we have used a parallelized version of v.surf.rst to effectively process massive datasets on multi-core computers using the OpenMP library (Hofierka et al., 2017b). Also, a lower spatial resolution of 5 m can be selected to further increase the speed of computation while still preserving relevant karst sinkholes. Setting the minimum distance between the input points for v.surf.rst to 5 m (the *dmin* parameter) we have efficiently reduced the number of input points used in the calculation of DEM to 2.1 million of points. The DEM was interpolated by the parallelized v.surf.rst on a standard desktop computer with four threads assigned to processor cores in 11 min. It represents all relevant land surface features with a great detail including sinkholes of various sizes (Fig. 4). The computing efficiency could be improved by decreasing the number of input points used for interpolation per each internal interpolation segment (the *npmin* parameter), but we used the default setting of 300 points. A lower value of *npmin* increases the probability of creation of

interpolation artefacts along the borders of the segments (Neteler and Mitasova, 2008).

### 3.2. Manual identification of sinkholes based on the ALS DEM, topographic maps and field surveys

Section 1 introduced several methods of identifying sinkholes with DEMs. While it is relatively unambiguous to locate sinkholes as points, delineating sinkholes as areal features can be approached from several aspects. In our approach, we tested several methods and parameters derived from the ALS DEM which could be useful for sinkholes identification. First, the hill-shaded elevation and mean curvature maps derived from the DEM (Mitášová and Hofierka, 1993) were visually inspected for oval local depression landforms which can potentially represent sinkholes. The sinkholes formed closed areas of negative mean curvature clearly delineated by zero values. Such features were preferentially sought within the extent of the large scale plateaux where the land surface is formed on carbonate bedrock and there are favourable conditions for formation of karst sinkholes. Two mutually perpendicular vertical profiles were drawn for each identified feature to check its cross-sectional shape. If the two 2-D profile lines formed a depression, the feature was delineated as a vector polygon object tracing its boundary as a line connecting the significant surface inflection points, i.e. transition between high and low slope angle values or change between

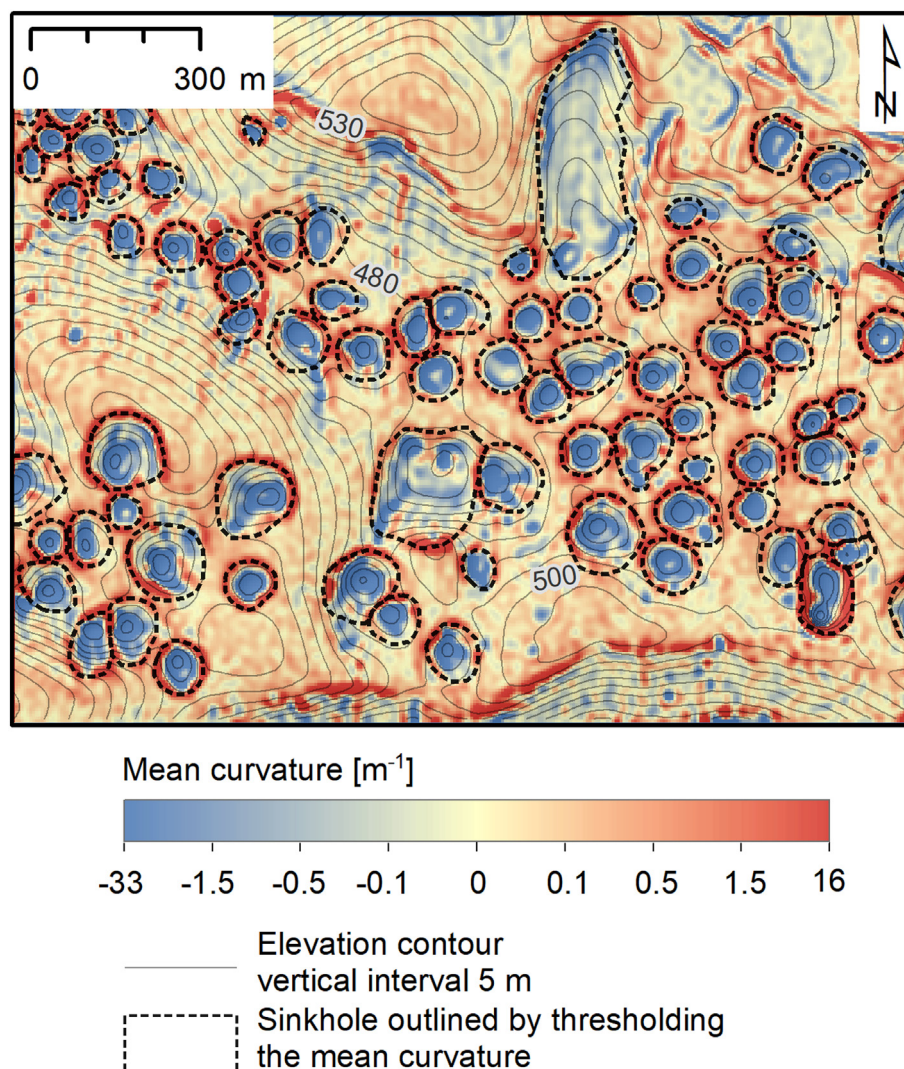


Fig. 5. Sinkholes identified manually using a hill-shaded mean curvature map and shaded relief map of the ALS DEM. The area is located in Fig. 1.



convex and concave profile curvature (Fig. 5). The sinkholes derived by this expert-driven method were used as the reference dataset in this study. With such a large study area and high number of sinkholes, it was not feasible to validate all reference sinkholes. However, we validated all of them using aerial orthoimagery and geological maps (Mello, 1996) to exclude real but unnatural sinkholes (e.g., those along roads or paths). Several field campaigns were undertaken in 2012–2016 in the surroundings of Silica, Kečovo, Dlhá Ves comprising about 20 km<sup>2</sup> where hand-held GPS receivers, topographic maps, and ALS derived maps were used to validate the topographic maps and also to minimize the occurrence of false positives in the reference dataset based on ALS.

Land surface depressions were delineated also by applying the DEM sink-filling method by Jenson and Domingue (1988) which is implemented by the *r.fill.dir* module in GRASS GIS (GRASS Development Team, 2017). We used the ALS DEM as input to the procedure. Initially, all the depressions were filled with one pass across the DEM. In the following step, the flow direction algorithm finds a unique direction for each cell. If it detects areas with potholes, it delineates this area from the rest of the area and once again the depressions are filled using the neighbourhood technique used by the flow direction routine. The final output resulted in a depressionless DEM which was subtracted from the original DEM to extract the depression layer.

Topographic maps are frequently used for identifying karst sinkholes and other geomorphologic features in regions where no ALS data are available such as Slovakia (Minár et al., 2001; Gessert, 2016). The method is based on identification of the outermost closed contour comprising the depression point. In this study, the topographic maps of 1:10,000 scale (GKÚ, 2002) were used to locate and delineate sinkholes by visual inspection and extraction of the outermost closed contour. The maps originated by photogrammetric surveying, therefore, the number of sinkholes is likely to be underestimated in the forested areas. The land surface height information on the maps is valid for the year of 2002. The vertical interval of contours was 2 m.

### 3.3. Process-based identification using a water flow model

The formation of karst sinkholes includes the process of water percolating through the soil and dissolving the underlying carbonate bedrock. During heavy rains or snow-thaw events the sinkhole may act as a funnel directing the water underground which is frequently observed by the inhabitants in the study area. Subsequently, a large amount of water may cause a development of underground spaces and caves. Especially during heavy rains, the rainfall rate may exceed the infiltration rate of the soil leading to rainfall excess and development of overland flow. There are numerous models representing the overland flow process (Wechsler, 2007; Shen et al., 2016). To assess the effects of surface water accumulating in the sinkholes, we have used the *r.sim.water* module of GRASS GIS which is part of the SIMWE model proposed by Mitas and Mitasova (1998). The water flow component of the SIMWE model has several advantages important for our study. It is a robust, flexible method based on the Monte Carlo simulation and diffusion-wave approximation of the Saint-Venant differential equations describing the overland flow (Mitasova et al., 2004). The key input parameters for the *r.sim.water* module include a grid-based DEM, water flow gradient (defined by the first-order partial derivatives of a DEM), rainfall excess rate and a surface roughness coefficient given by the Manning's *n*. The outputs include grid-based maps of water depth (m), and water discharge (m<sup>3</sup> s<sup>-1</sup>) (Fig. 6).

The module uses a modifiable diffusion term parameter which enables water flow to overcome shallow DEM surface depressions or obstacles when water depth exceeds a threshold water depth value. After this, threshold value is reached, the diffusion term increases by a chosen value and the water flow continues in a more diffusion-like movement (Hofierka and Knutová, 2015; Jeziorska et al., 2016). This feature makes the method more stable and realistic especially in land surface depressions or various flow obstacles. The simulation is computationally very robust; it does not need any data editing such as depression elimination, which is frequent in other approximation

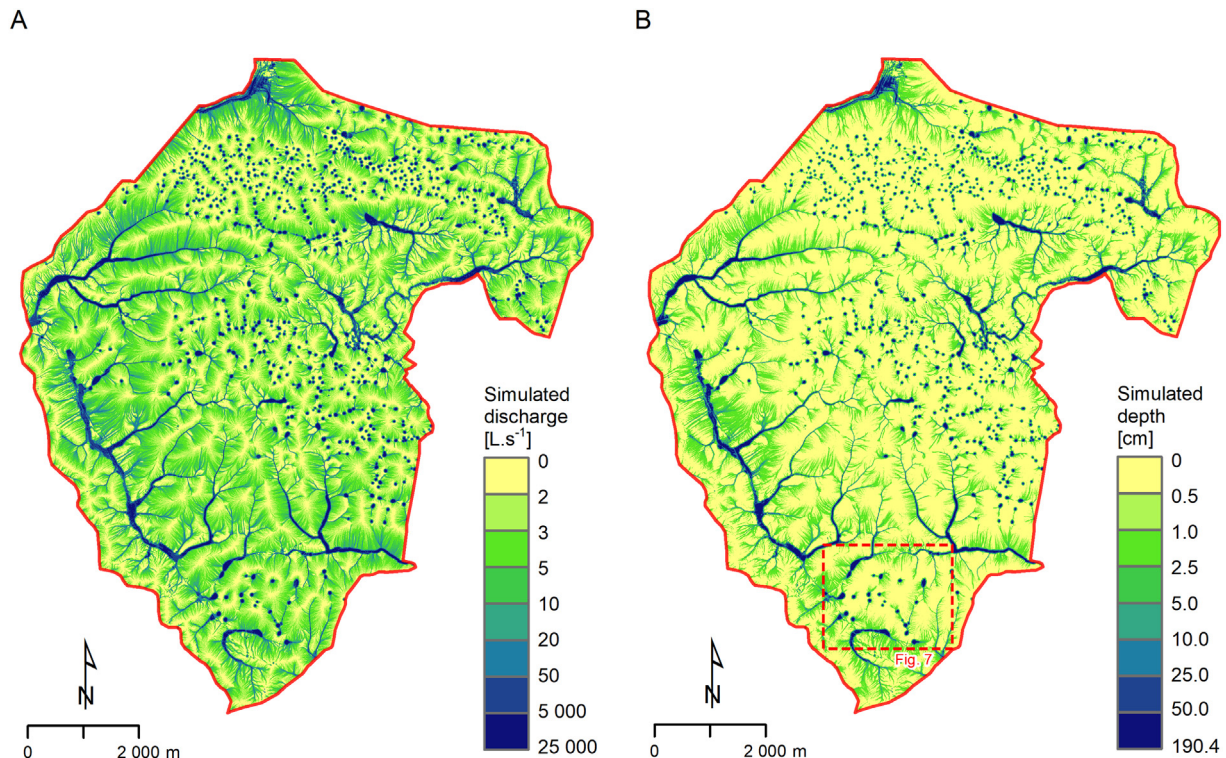


Fig. 6. Grid-based map of water discharge (A) and water depth (B) of the simulated water flow. The red dashed rectangle delineates the area shown in Fig. 7.

**Table 2**

Summary of sinkholes identified by the four different approaches for the whole study area and for the carbonate bedrock only.

Row	Observed variable	(1) Topo map	(2) DEM sink-fill	(3) Water flow simulation	(4) Manual DEM inspection (reference sinkholes)
A	Number of all sinkholes (count)	472	1618	956	664
B	Number of sinkholes on carbonate bedrock (count)	432	657	592	622
C	Number of sinkholes on carbonate bedrock intersecting with the reference (count)	420	525	562	622
D	B/C = True positives (%) (ratio of found karst sinkholes out of all found sinkholes by the method)	97	80	95	100
E	(B – C)/B = False positives (%) (ratio of sinks not being real karst sinkholes out of all found sinkholes by the method)	3	20	5	0
F	C/reference B = Found true positives (%) (ratio of found reference karst sinkholes out of all reference karst sinkholes)	68	84	90	100
G	(reference B – C)/reference B = Missing true positives (%) (ratio of missing reference karst sinkholes out of all reference karst sinkholes)	32	16	10	0

methods. It is able to fill-up depressions and overflow them in a controllable way.

Default parameters of the *r.sim.water* module were used to keep the modelling as simple as possible, but within a realistic scenario. This setting assumes a uniform rainfall excess rate (rainfall – infiltration) of 50 mm hour<sup>−1</sup> and Manning's *n* of 0.1 for overland flow (equivalent to grassland). With the duration of 120 min, we simulated a long, heavy rainfall event that should produce a strong, near steady-state overland flow. Such conditions were recorded several times over the last hundred years of modern meteorological measurement in the study area. It can be assumed that such heavy rainfall events also occurred during the Quaternary considerably contributing to the formation of sinkholes. The DEM was the only spatially variable data and this makes it comparable to the other two methods which are based on the DEM properties.

Gradient field (slope angle) of the water discharge grid data layer was calculated via the *r.slope.aspect* module in order to define the outer boundaries of the sinkholes where the water accumulated, and the value of 15 was used to extract the sinkhole boundaries. We selected

the threshold gradient value by trial-and-error approach, which was the most suitable for the study area. Different threshold values would cause either less significant sinks or missing significant sinks. The gradient value of 15 located only the large (significant) depression features. We used the *r.stats.zonal* module to calculate the amount of water accumulated during the simulated rainfall event in karst sinkholes as polygons delineated by the manual method (Section 3.2).

#### 4. Results and discussion

Four different approaches were used to identify sinkholes from the ALS-based DEM and topographic maps. First, we summarise the results for the entire extent of the study area (Table 2, row A). The method based on identification of the outermost closed contour from topographic maps (Method 1) located 472 sinks; DEM sink-filling approach (Method 2) identified 1618 sinks; and the process-oriented method based on water flow simulation (Method 3) found 956 sinks. These findings can be compared with Method 4 based on manual DEM inspection

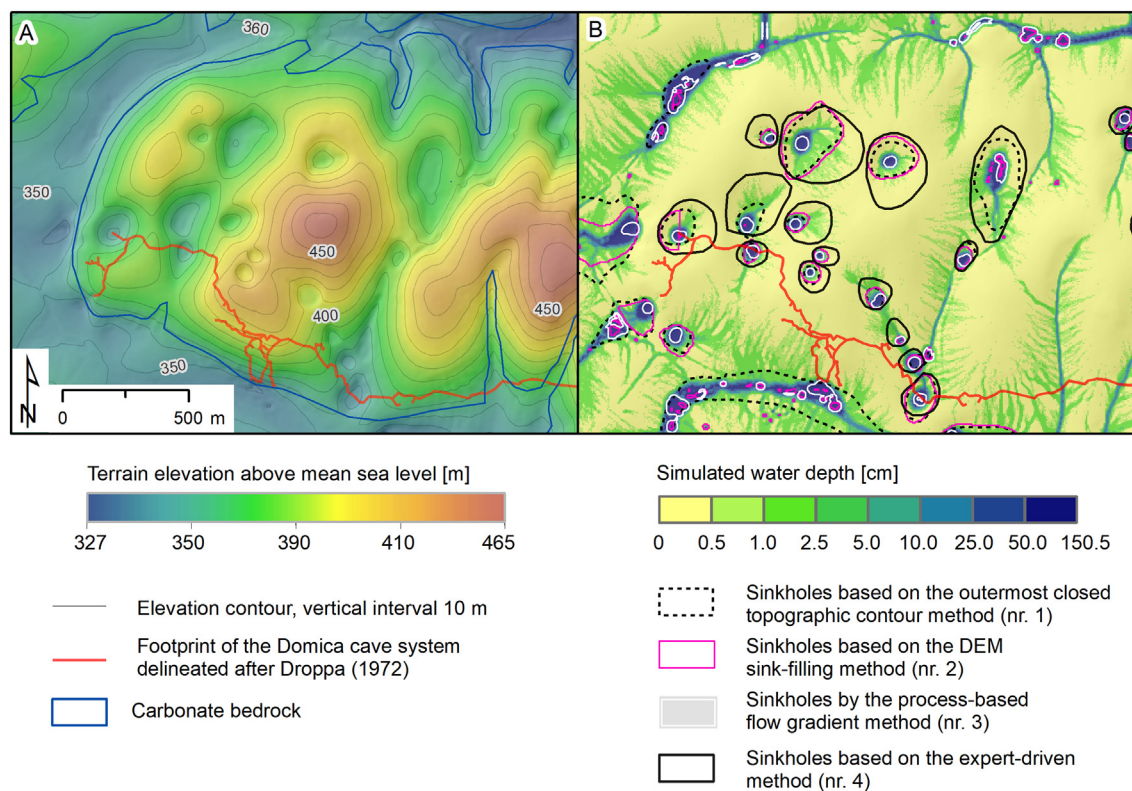


**Fig. 7.** Maps of hill-shaded elevation (A) and delineated sinkholes and water flow depth at the end of the simulated rainfall (B), along with the distribution of the Domica cave system delineated after Droppa (1972). (A) is also overlaid with the outline of the carbonate bedrock. (B) shows outlines of sinkholes delineated by four different methods. The location of the area is shown in Fig. 6.



**Table 3**  
Summary of sinkhole areas for the carbonate bedrock from the four different methods.

Statistics	(1) Topo map	(2) DEM sink-fill	(3) Water flow simulation	(4) Manual DEM inspection (reference sinkholes)
Count	432	657	592	622
Min (ha)	0.011	0.003	0.018	0.032
Max (ha)	46.545	5.835	0.776	10.715
Mean (ha)	4.398	0.3952	0.116	0.913
St. deviation (ha)	5.474	0.5416	0.0574	0.92
Total area (ha)	189.588	259.658	72.029	569.987

and vectorizing of polygons enclosing the sinkholes using the mean curvature and shaded relief maps, which provided the reference dataset for this research (Fig. 3). Method 4 resulted in 664 natural surface depressions of which 92% is covered by forest. When comparing the number of all reference sinkholes with other methods (Table 2), it is clear that Method 1 underestimates the number of depressions which can be attributed to the high percentage of the land covered by forests. Method 2 identified more than twice as many sinkholes as the reference count mainly due to the excessive sensitivity of the method to detect sinks including artificial ones generated by DEM interpolation. The overestimation is less for Method 3 because of simulated water flow over the DEM surface that leads to filling of small and frequent artificial DEM sinks.

Thus, Method 3 showed promising potential to remove artificial DEM sinks generated by DEM interpolation or low-amplitude natural undulation of the land surface, which are not genetically related to the formation of karst sinkholes. However, real but unnatural depressions are still involved in the result. Therefore, manual expert-driven judgement is needed to differentiate the karst depressions.

The differences among the applied methods are mapped for the southern part of the study area (Fig. 7) in the surrounding of the Domica cave and at the boundary of the carbonate bedrock. There are dramatic differences in sinkhole size and boundary according to methods. In particular, a considerable number of sinkholes along the streams were detected by Methods 2 and 3 (Fig. 7B). Such sinks along streams are either (i) small-scale features (e.g., DEM errors), (ii) induced by human interference with land surface, or (iii) ponors comprised within a much larger depression from combined fluvial-corrosional processes. Such sinks were excluded from the further analysis and we focused on karst sinkholes. The karst sinkholes (622) encompassed 94% of the reference sinkholes (664). The majority of the reference sinkholes are covered with forest (96%). The number of identified sinkholes on carbonate bedrock and their spatial intersection with the reference sinkholes are shown in Table 2 (rows B and C) and the accuracies as percentages are also reported (Rows D–G). The internal accuracy of Method 1 was the highest (97% of true positives) but it missed 32% of all reference karst sinkholes. Out of the 202 missing reference polygons (Table 2,

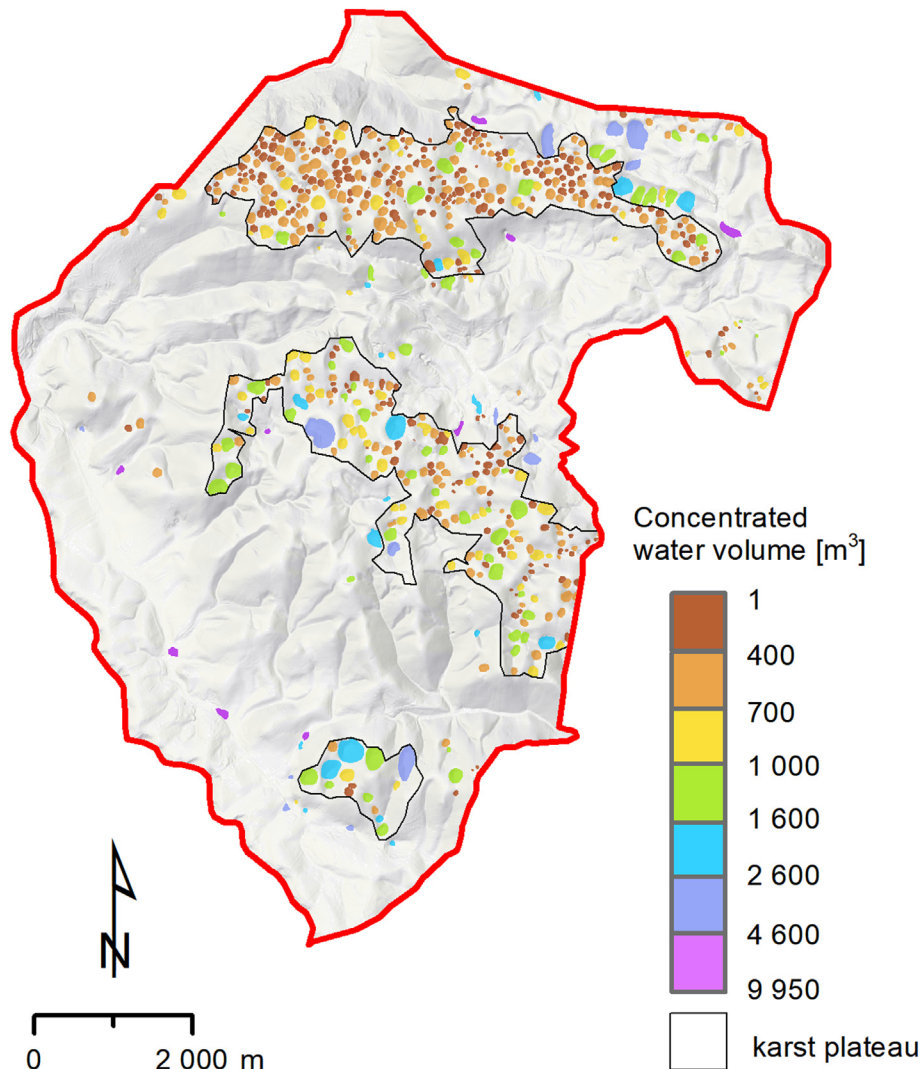


**Fig. 8.** Accumulation of water in sinkholes estimated from water flow depth simulated by the *r.sim.water* module.

row C), 194 polygons (96%) were located under forest canopy which explains why there were not captured during the production of the topographic contours. The accuracy of Method 3 based on water flow was slightly lower (95%) but it located 90% of all reference polygons on carbonate bedrock. Method 2 achieved the lowest rate of true positives (84%) and the second lowest rate of missed true positives (16%).

The summary of area of karst sinkholes is presented in Table 3. The total extent of the reference karst sinkholes is about 570 ha. The total area for Methods 1–3 is much smaller than the total area of the reference dataset; even the best performing method (2) has the total area lower than the half of the reference polygons. The mean area of karst sinkholes from Method 1 are more than four times larger than the reference value. The sinkhole area from Method 3 is unsuitable because the delineated polygons tend to be much smaller than the reference. This limitation is not surprising as the method focuses on locating the sink bottom. Also the boundary of a sinkhole is often fuzzy and its delineation depends on the parameterisation of the hydrologic model and the purpose of mapping.

It should be noted that spatially differentiated Manning's  $n$  values based on the real land cover would improve the resulting water depth values of overland flow at the end of the simulated rainfall event. However, the main purpose of this study was relative differentiation between the sinkholes according to their influence on water flow for which, we believe setting a uniform  $n$  value of 0.1 is acceptable. The correlation between the contemporary land surface morphology and the contemporary land cover is likely not to be strong. While the karst landscape evolved over thousands of years or even millions of years, the land cover has markedly changed several times over the last two centuries which was induced by human activity (Olah et al., 2009). Also natural alterations of the vegetation cover occurred several times in the earlier Holocene.

The amount of accumulated water in sinkholes is shown in Fig. 8. The amount of water depends on the sinkhole catchment area and therefore it is not purely a function of the sinkhole size. If a large amount of water flows into a sinkhole, we can assume that it contributes to the development of the underground fluvial system and consequently to the development of caves. The presence of large sinkholes close to the

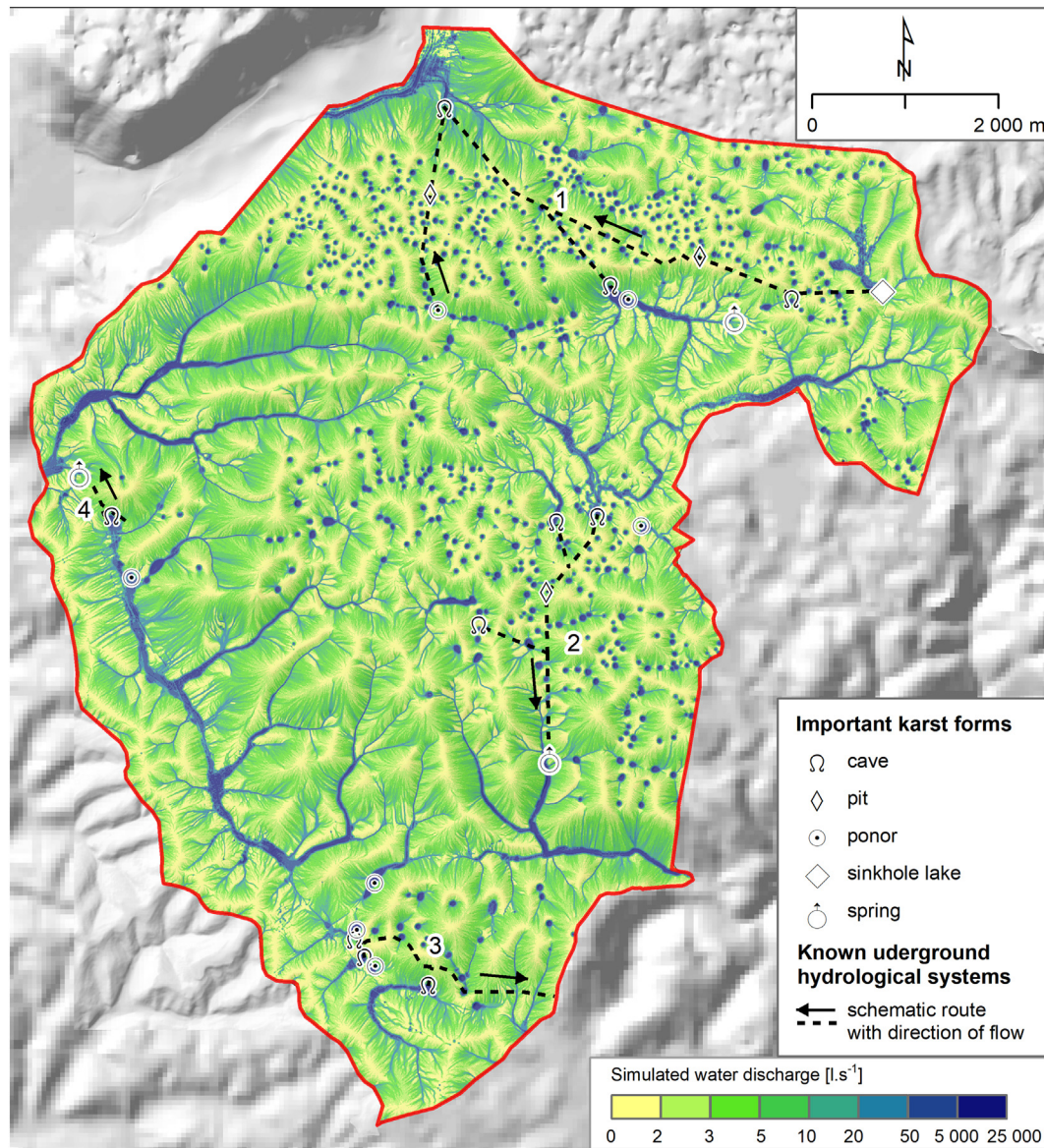


**Fig. 9.** Simulated water flow discharge (see Fig. 6A for the legend) overlaid with important karst forms known to be related with underground hydrological systems according to Hochmuth (2008) and Gaál (2008): (1) Silica-Gombasek system with the Majkova cave, (2) the Brezovsko-kečovský system, (3) the Domica-Baradla cave system, and (4) the Ardovská cave system.



Domica cave indicates that karst areas covered by sinkholes with high water accumulation capacity may lead to the development of larger caves. The study area comprises about a half of the Silická planina Plateau where Hochmuth (2008) reports 288 caves.

The sinkholes identified by all methods are concentrated in three distinct areas (Fig. 8). The northern strip contains many smaller sinkholes. This area is almost completely covered by dense forest. The height of trees is around 30–40 m (Fig. 3). According to the water flow analysis during the simulated rainfall event, every square meter of a sinkhole accumulates  $39.64 \text{ m}^3$  of water on average. The average size of sinkholes is 0.76 ha. The central strip contains a mixture of large and small sinkholes with an average size is 0.98 ha. The vegetation canopy consists of patches of younger forests and shrubs with various densities and heights (3–20 m). Every square meter of sinkholes in this area accumulates  $47.42 \text{ m}^3$  of water on average. The smallest, southern strip is associated with the Domica cave system. It contains several large sinkholes, most of them covered by forest and shrubs. The density and height of vegetation canopy is lower than within the previous two groups (3–12 m). Every square meter of sinkholes in this area accumulate  $142.43 \text{ m}^3$  of water on average and the average size of sinkholes is 1.71 ha. Several large sinkholes in this area are close to each other and the simulation of a heavy rainfall event showed that each of the sinkholes can concentrate volume of several thousands  $\text{m}^3$  of water per hour that can flow in a concentrated form into the underground system of the Styx river that drains the main corridor of the Domica cave system. The size of sinkholes and their accumulated volume of water tend to increase from the north to the south of the area. It can be associated with the depth of the phreatic zone which also decreases from

the north (ca. 100 m) to the south (a few m), i.e., smaller sinkholes are associated with a thicker vadose zone.

The simulation revealed presence of depressions such as ponors which are not only related to dissolution of carbonate rocks but also to the formation of superficial and underground drainage network. In comparison with the sinkholes formed on carbonate bedrock, these land surface depressions are situated at the foothills of plateaux thus being at a relatively lower vertical position. They are hierarchically higher order forms and they had become likely to be formed much earlier than sinkholes up on the plateaux. Fig. 9 shows the well-known and most important sinkholes related to four known underground hydrological systems in the study area. Their existence was proved by water dyeing tests and cave surveying. The underground routes are outlined according to Hochmuth (2008) and Gaál (2008) who summarized the related research and they thoroughly described the hydrological settings in Slovak Karst. The pattern of the simulated overland water flow (Fig. 9) clearly shows the extent of the area contributing to the concentration of water in the ponors and caves. For example, the contemporary superficial drainage of the ponors related to the Domica-Baradla cave system (3) is relatively small; however, the cave volume and size of the cave corridors suggest that the underground water flow had to be much stronger than the contemporary stream of Styx which drains the Domica cave (Droppa, 1972; Bella and Bosák, 2015). Cosmogene dating of burial age of quartz gravels in the cave (Bella et al., 2014) also indicates much older dates of cave formation in the Upper Pliocene than previously expected dates in the Quaternary. It is hypothesized that main erosion effect of the underground Styx stream occurred during extreme events and not during normal

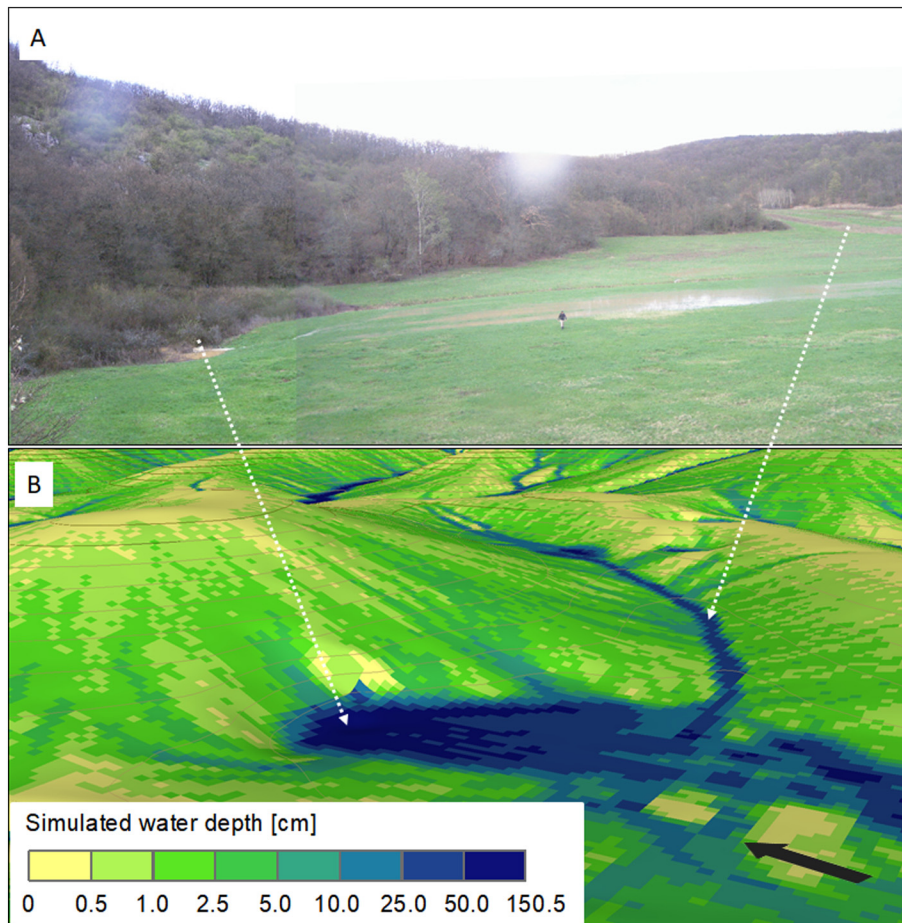


**Fig. 10.** Comparison of a real rainfall event observed on 15 April 2010 (A) and simulated water flow depth (B) in the area of the Ardovska cave ponor indicated by white arrows (system 4 in Fig. 9). The black arrow indicates north direction. Elevation contours are indicated with brown lines of 10 m vertical interval. The simulated water flow depth map is draped over the lidar DEM (B). Photograph is by Ľubomír Kováč.

discharges which are nowadays low  $1\text{--}2\text{ L s}^{-1}$  while they can reach 120 L s during snow-thaw or extreme rainfalls (Haviarová and Gruber, 2014). Such an event from February 2016 is reported by Hochmuth and Gessert (2016) when the environmental conditions were similar to those simulated in the presented research. This particular event implies that such similar environmental circumstances used to be either more frequent or stronger throughout the cave formation in the past. Fig. 10A demonstrates how overland flow was concentrated during a heavy rainfall in spring 2010 in the ponor of the Ardovská cave (system 4 in Fig. 9) and water depth after the simulated rainfall event (Fig. 10B).

## 5. Conclusions

Modern data collection methods such as laser scanning produce massive 3D datasets containing billions of points which represent landscape features with unprecedented spatial detail and measurement accuracy. They help to identify even relatively small geomorphological features such as sinkholes under dense forest canopy or in poorly accessible terrain. Airborne lidar enables mapping sinkholes under forest canopy even under leaf-on conditions given sufficient point density is used for laser scanning. The dense point cloud reduces the likelihood of artificial depressions of a digital land surface originating in the interpolation of a grid-based DEM. Therefore, such depressions are eliminated and only depressions really existing in the terrain remain. Differentiating between karst sinkholes and other depressions (e.g. ponors, and man-made depressions) requires field check, expertise, or auxiliary data.

We tested several methods for sinkhole mapping. Each of them yielded a different number and different areal extent of sinkholes ultimately requiring expert knowledge and auxiliary data to identify the real karst depressions. The approach based on overland flow simulation is suitable for locating the sinkholes as features which concentrate surficial water flow. Sinkholes can be delineated by manual approach or any other approach (sink-filling) but using the presented technique these sinkholes can be better identified and differentiated based on the volume of water flow concentrated by the sinkholes. This also helps to better understand the importance of sinkholes for subsurface flow generation and subsequent cave development.

The advantage of the presented process-based approach over other sinkhole mapping techniques consists in means for assessing the relative magnitude of sinkholes in terms of their hydrologic function and its relation to the underground karst, i.e., how overland hydrological processes affect the underground hydrology. If the absolute amount of water is the main objective, soil and land cover variables such as surface roughness or infiltration rate have to be more accurately specified in the water flow simulation.

Future research can focus on modelling the effect of contemporary land cover on defining the absolute amount of water for particular rainfall events or the prediction of scenarios under a certain type of rainfall events. Simultaneous monitoring of weather parameters or hydrological water discharge could provide reference data to validate the accuracy of such prediction.

## Acknowledgement

This work originated within the research projects APVV-0176-12 and APVV-15-0054 supported by the Slovak Research and Development Agency and VEGA 1/0474/16 and VEGA 1/0963/17 supported by the Slovak Research Grant Agency VEGA. We would like to thank our colleagues Ľubomír Kováč of the Institute of Biology and Ecology, P.J.Šafárik University in Košice for providing the photographs of a rainfall event near the Ardovská cave for this research.

## Appendix A. Supplementary data

Supplementary data associated with this article can be found in the online version at <https://doi.org/10.1016/j.geomorph.2018.02.004>.

These data include the Google map of the most important areas described in this article.

## References

- Alexander, S.C., Rahimi, M., Larson, E., Bomberger, C., Greenwaldt, B., Alexander Jr., E.C., 2013. Combining LiDAR, aerial photography and pictometric tools for karst features database management. In: Land, L., Doctor, D.H., Stephenson, J.B. (Eds.), NCKRI Symposium 2 Proceedings of the 13th Multidisciplinary Conference on Sinkholes and the Engineering and Environmental Impacts of Karst, Carlsbad, New Mexico, Published on-Line by NCKRI, Carlsbad, NM, pp. 441–448.
- Angel, J.C., Nelson, D.O., Panno, S.V., 2004. Comparison of a new GIS-based technique and a manual method for determining sinkhole density: an example from Illinois' sinkhole plain. *J. Cave Karst Stud.* 66, 9–17.
- Antonic, O., Hatic, D., Pernar, R., 2001. DEM-based depth in sink as an environmental estimator. *Ecol. Model.* 138, 247–254.
- Balogh, M., Barabas, D., 2016. Analysis of species composition of tree cover in the area of Slovak Karst (Slovenský kras). *Geogr. Cassoviensis* 10, 93–106 (in Slovak).
- Barabas, D., Gallay, M., Petrvalská, A., 2010. The use and importance of digital geomorphometry for understanding the development of the superficial depression forms in the area of Palanta (Jasovská Plateau). *Slovenský kras: Acta Carsologica Slovaca* 48, 253–261 (in Slovak).
- Bátori, Z., Csiky, J., Farkas, T., Vojtkó, A.E., Erdős, L., Kovács, D., Wirth, T., Körmöczi, L., Vojtkó, A., 2014. The conservation value of karst dolines for vascular plants in woodland habitats of Hungary: refugia and climate change. *Int. J. Speleol.* 43:15–26. <https://doi.org/10.5038/1827-806X.43.1>.
- Bauer, C., 2015. Analysis of dolines using multiple methods applied to airborne laser scanning data. *Geomorphology* 250, 78–88.
- Bella, P., 2001. Geomorphological settings of the Domica Cave. *Aragonit* 3, 5–11.
- Bella, P., Bosák, P., 2015. Ceiling erosion in caves: early studies and Zdeněk Roth as author of the concept. *Acta Carsologica* 44:139–144. <https://doi.org/10.3986/ac.v44i1.768>.
- Bella, P., Braucher, R., Holec, J., Veselský, M., 2014. Datovanie pochovania kremiteho štrku na vrchnej vývojovej úrovni jaskyne Domica pomocou kozmogénnych nuklidov. *Acta Carsologica Slovaca* 52, 15–24 (in Slovak).
- Bishop, M.P., James, L.A., Shroder Jr., J.F., Walsh, S.J., 2012. Geospatial technologies and digital geomorphological mapping: concepts, issues and research. *Geomorphology* 137, 5–26.
- de Carvalho Júnior, O.A., Guimarães, R.F., Montgomery, D.R., Gillespie, A.R., Trancoso Gomes, R.A., de Souza Martins, E., Silva, N.C., 2014. Karst depression detection using ASTER, ALOS/PRISM and SRTM-derived digital elevation models in the Bambuí Group, Brazil. *Remote Sens.* 6:330–351. <https://doi.org/10.3390/rs6010330>.
- Development Team, G.R.A.S.S., 2017. Geographic Resources Analysis Support System (GRASS) Software, Version 7.0. Open Source Geospatial Foundation. [Online]. <http://grass.osgeo.org> (January 2017).
- Doctor, D.H., Young, J.A., 2013. An evaluation of automated GIS tools for delineating karst sinkholes and closed depressions from 1-meter lidar-derived digital elevation data. In: Land, L., Doctor, D.H., Stephenson, J.B. (Eds.), Sinkholes and the Engineering and Environmental Impacts of Karst: Proceedings of the Thirteenth Multidisciplinary Conference, May 6–10, Carlsbad, New Mexico: NCKRI Symposium 2. National Cave and Karst Research Institute, Carlsbad (NM), pp. 449–458.
- Droppa, A., 1972. Contribution to the evolution of the Domica cave. *Československý kras* 22, 65–72 (in Slovak).
- Farrant, A., Cooper, A., 2008. Karst geohazards in the UK: the use of digital data for hazard management. *Q. J. Eng. Geol. Hydrogeol.* 41:339–356. <https://doi.org/10.1144/1470-9236/07-201>.
- Ford, D.C., Williams, P., 2007. *Karst Hydrogeology and Geomorphology*. Wiley, Chichester.
- Gaál, Ľ., 2008. Geodynamika a vývoj jaskýň Slovenského krasu (Geodynamics and evolution of caves in Slovak Karst). *Speleologia Slovaca* 1. Liptovský Mikuláš, Slovakia, Štátna ochrana prírody SR (in Slovak).
- Gaállová, B., Donauerová, A., Seman, M., Bujdaková, H., 2014. Identification and  $\beta$ -lactam resistance in aquatic isolates of *Enterobacter cloacae* and their status in microbiota of Domica Cave in Slovak Karst (Slovakia). *Int. J. Speleol.* 43, 69–77.
- Gallay, M., Kaňuk, J., Hochmuth, Z., Meneely, J.D., Hofierka, J., Sedlák, V., 2015. Large-scale and high-resolution 3-D cave mapping by terrestrial laser scanning: a case study of the Domica Cave, Slovakia. *Int. J. Speleol.* 44, 277–291.
- Gallay, M., Hochmuth, Z., Kaňuk, J., Hofierka, J., 2016. Geomorphometric analysis of cave ceiling channels mapped with 3D terrestrial laser scanning. *Hydrol. Earth Syst. Sci.* 20:1827–1849. <https://doi.org/10.5194/hess-20-1827-2016>.
- Gao, Y., Alexander, E.C., Tipping, R., 2002. The development of a karst feature database for southeastern Minnesota. *Journal of Cave and Karst Studies* 64, 51–57.
- Gessert, A., 2016. Geomorphology of the Slovak Karst (eastern part). *Journal of Maps* 12: 285–288. <https://doi.org/10.1080/17445647.2016.1202874>.
- GKÚ, 2002. Základná mapa Slovenskej republiky 1: 10 000 – WMS service. Geodetický a kartografický ústav Slovenskej republiky, Bratislava.
- Gutiérrez, F., Galve, J.P., Lucha, P., Castañeda, C., Bonachea, J., Guerrero, J., 2011. Integrating geomorphological mapping, trenching, InSAR and GPR for the identification and characterization of sinkholes: a review and application in the mantled evaporite karst of the Ebro Valley (NE Spain). *Geomorphology* 134, 144–156.
- Gutiérrez, F., Parise, M., De Waele, J., Jourde, H., 2014. A review on natural and human-induced geohazards and impacts in karst. *Earth Sci. Rev.* 138:61–88. <https://doi.org/10.1016/j.earscirev.2014.08.002>.
- Haviarová, D., Gruber, P., 2014. Voda v krase (Water in the karst). In: Gaál, Ľ., Gruber, P. (Eds.), Jaskynný systém Domica-Baradla jaskyňa, ktorá nás spája (The Domica – Baradla Cave System, the Cave Which Connects Us). Aggteleki Nemzeti Park Igazgatóság: Jósvalő, Hungary, pp. 185–210 (in Slovak).



- Geomorphometry: concepts, software, applications. In: Hengl, T., Reuter, H.I. (Eds.), *Developments in Soil Science*. vol. 33. Elsevier.
- Hochmuth, Z., 2008. Krasové územia a jaskyne Slovenska (Karst areas and caves in Slovakia). *Geographia Cassoviensis* 2, 1–210 (in Slovak).
- Hochmuth, Z., Gessert, A., 2016. Floods in Domica and hydraulic pulse. *Bull. Slovak Speleol. Soc.* 47, 30–33 (in Slovak).
- Hofierka, J., Knutová, M., 2015. Simulating spatial aspects of a flash flood using the Monte Carlo method and GRASS GIS: a case study of the Malá Svinka Basin (Slovakia). *Open Geosci.* 7, 118–125.
- Hofierka, J., Gallay, M., Kaňuk, J., 2013. In: Buchroithner, M.F. (Ed.), *Spatial Interpolation of Airborne Laser Scanning Data with Variable Data Density*. Proceedings of the 26th International Cartographic Conference, August 25–30, 2013, Dresden Germany.
- Hofierka, J., Gallay, M., Kaňuk, J., Šašák, J., 2017a. Modelling Karst landscape with massive airborne and terrestrial laser scanning data. In: Ivan, I., Singleton, A., Horák, J., Inspektor, T. (Eds.), *The Rise of Big Spatial Data, Lecture Notes in Geoinformation and Cartography*. Springer International Publishing, pp. 141–154 [https://doi.org/10.1007/978-3-319-45123-7\\_11](https://doi.org/10.1007/978-3-319-45123-7_11).
- Hofierka, J., Lacko, M., Zubal, S., 2017b. Parallelization of interpolation, solar radiation and water flow simulation modules in GRASS GIS using OpenMP. *Comput. Geosci.* 107, 20–27.
- Isenburg, M., 2014. LAStools - Efficient LiDAR Processing Software (Version 140117, Unlicensed), obtained from <http://rapidlasso.com/LAStools> (November 2015).
- Jakál, J., 1975. Kras Silickej planiny (The karst of the Silická planina Plateau). *Osveta: Martin, Czechoslovakia* (in Slovak).
- Jakál, J., Feranec, J., Harčár, J., Lacika, J., Urbánek, J., 1992. Využitie radarových záznamov v geomorfologii. (Using of radar images in geomorphology). *Miner. Slovaca* 24, 257–270 (in Slovak).
- James, L.A., Watson, D.G., Hansen, W.F., 2007. Using LiDAR data to map gullies and headwater streams under forest canopy: South Carolina, USA. *Catena* 71:132–144. <https://doi.org/10.1016/j.catena.2006.10.010>.
- Jenson, S.K., Domingue, J.O., 1988. Extracting topographic structure from digital elevation model data for geographic information system analysis. *Photogramm. Eng. Remote Sens.* 54, 1593–1600.
- Jeziorska, J., Mitasova, H., Petrasova, A., Petras, V., Divakaran, D., Zajkowski, T., 2016. Overland flow analysis using time series of sUAS-derived elevation models. *ISPRS Ann. Photogramm. Remote Sens. Spatial Inf. Sci.* III-8:159–166. <https://doi.org/10.5194/isprs-annals-III-8-159-2016>.
- Kobal, M., Bertoncelj, I., Pirotti, F., Dakschobler, I., Kutnar, L., 2015. Using Lidar data to analyse sinkhole characteristics relevant for understory vegetation under Forest cover – case study of a high karst area in the Dinaric Mountains. *PLoS One* 10, e0122070. <https://doi.org/10.1371/journal.pone.0122070>.
- Kováč, L., Elhotová, D., Mock, A., Nováková, A., Krištúfek, V., Chroňáková, A., Lukešová, A., Mulec, J., Košel, V., Papáč, V., Luptáčík, P., Uhrin, M., Višňovská, Z., Hudec, I., Gaál, I., Bella, P., 2014. The cave biota of Slovakia. *Speleologia Slovaca* 5. State Nature Conservancy SR, Slovak Caves Administration, Liptovský Mikuláš.
- Li, S., MacMillan, R.A., Lobb, D., Earle, T.J., McNabb, D.H., 2011. Lidar DEM error analyses and topographic depression identification in a hummocky landscape in the Prairie Region of Canada. *Geomorphology* 129:263–275. <https://doi.org/10.1016/j.geomorph.2011.02.020>.
- Lindsay, J.B., Creed, I.F., 2006. Distinguishing actual and artefact depressions in digital elevation data. *Comput. Geosci.* 32, 1192–1204.
- Luman, D.E., Panno, S.V., 2013. Mapping palimpsest karst features on the Illinois sinkhole plain using historical aerial photography. *Carbonate Evaporites* 28:201–214. <https://doi.org/10.1007/s13146-012-0107-4>.
- MacMillan, R.A., Martin, T.A., Earle, T.J., McNabb, D.H., 2003. Automated analysis and classification of landforms using high-resolution digital elevation data: applications and issues. *Can. J. Remote. Sens.* 29:592–606. <https://doi.org/10.5589/m03-031>.
- Mello, J., 1996. Geological Map of the Slovak Karst 1:50 000. Geologická služba Slovenskej republiky, Bratislava (in Slovak).
- Minár, J., Barka, I., Bonk, R., Bízubová, M., Čerňanský, J., Falt'an, V., Gašpárek, J., Kolény, M., Kožuch, M., Kusendová, D., Machová, Z., Mičian, L., Mičietová, E., Michalka, R., Novotný, J., Ružek, I., Švec, P., Tremboš, P., Trizna, M., Zát'ko, M., 2001. Geoeologický (geoeologický fyzikogeografický) výskum a mapovanie vo veľkých mierkach (Geoeological (complex physical geographical) research and mapping in large scales). *Geografické spektrum*. 3. Bratislava, Slovakia, Geo-grafika.
- Minár, J., Bielik, M., Kováč, M., Plašienka, D., Barka, I., Stankoviánsky, M., Zeyen, H., 2011. New morphostructural subdivision of the Western Carpathians: an approach integrating geodynamics into targeted morphometric analysis. *Tectonophysics* 502, 158–174.
- Mitáš, L., Mitášová, H., 1993. Interpolation by regularized spline with tension: I. Theory and implementation. *Math. Geol.* 25:641–655. <https://doi.org/10.1007/BF00893171>.
- Mitas, L., Mitasova, H., 1998. Distributed soil erosion simulation for effective erosion/deposition modeling and enhanced dynamic visualization. *Water Resour. Res.* 34, 505–516.
- Mitášová, H., Hofierka, J., 1993. Interpolation by regularized spline with tension: II. Application to terrain modeling and surface geometry analysis. *Math. Geol.* 25: 657–669. <https://doi.org/10.1007/BF00893172>.
- Mitasova, H., Thaxton, C., Hofierka, J., McLaughlin, R., Moore, A., Mitas, L., 2004. Path sampling method for modeling overland water flow, sediment transport and short term terrain evolution in Open Source GIS. In: Miller, C.T., Farthing, M.W., Gray, V.G., Pinder, G.F. (Eds.), *Proceedings of the XVth International Conference on Computational Methods in Water Resources (CMWR XV)*. 2004. Elsevier, Chapel Hill, NC, USA, pp. 1479–1490 June 13–17 2004.
- Mitasova, H., Mitas, L., Harmon, R.S., 2005. Simultaneous spline approximation and topographic analysis for lidar elevation data in open-source GIS. *IEEE Geosci. Remote Sens. Lett.* 2:375–379. <https://doi.org/10.1109/LGRS.2005.848533>.
- Neteler, M., Mitasova, H., 2008. Open Source GIS: a GRASS GIS approach. *The International Series in Engineering and Computer Science, Third Edition Volume 773*. Springer, New York.
- Neteler, M., Bowman, M.H., Landa, M., Metz, M., 2012. GRASS GIS: a multi-purpose open source GIS. *Environ. Model. Softw.* 31:124–130. <https://doi.org/10.1016/j.envsoft.2011.11.014>.
- Obu, J., Podobnikar, T., 2013. Algorithm for karst depression recognition using digital terrain models. *Geodetski Vestnik* 57, 260–270.
- Olah, B., Boltziar, M., Gallay, I., 2009. Transformation of the Slovak cultural landscape since the 18th cent. and its recent trends. *J. Landsc. Ecol.* 2, 41–55.
- PaDCNP, 2016. Interactive Map of Sinkholes. Pennsylvania Department of Conservation and Natural Resources. <http://www.gis.dcnr.state.pa.us/maps/index.html?geology=true>.
- Panno, S.V., Weibel, C.P., 1996. Karst regions of Illinois: Illinois state geological survey. *Open File Series* 2 (42 p).
- Pardo-Igúzquiza, E., Valsero, J.J.D., Dowd, P.A., 2013. Automatic detection and delineation of karst terrain depressions and its application in geomorphological mapping and morphometric analysis. *Acta Carsologica* 42:17–24. <https://doi.org/10.3986/ac.v42i1.637>.
- Pipaud, I., Loibl, D., Lehmkuhl, F., 2015. Evaluation of TanDEM-X elevation data for geomorphological mapping and interpretation in high mountain environments – a case study from SE Tibet, China. *Geomorphology* 246:232–254. <https://doi.org/10.1016/j.geomorph.2015.06.025>.
- Rozložník, M., 1998. The biosphere reserve Slovak Karst/Slovenský kras from the viewpoint of its twenty years existence. *Životné prostredie* 32, 15–18 (in Slovak).
- Schlund, M., von Poncet, F., Kuntz, S., Schumliuss, C., Hoekman, D.H., 2015. TanDEM-X data for aboveground biomass retrieval in a tropical peat swamp forest. *Remote Sens. Environ.* 158:255–266. <https://doi.org/10.1016/j.rse.2014.11.016>.
- Seale, L.D., Florea, L.J., Vacher, H.L., Brinkmann, R., 2008. Using ALSM to map sinkholes in the urbanized covered karst of Pinellas County, Florida—1, methodological considerations. *Environ. Geol.* 54, 995–1005.
- Shadem, B.L., Alexander Jr., E.C., Alexander, S.C., 2013. In: Land, L., Doctor, D.H., Stephenson, J.B. (Eds.), *The Sandstone Karst of Pine County, Minnesota*. NCKRI Symposium 5 Proceedings of the 14th Multidisciplinary Conference on Sinkholes and the Engineering and Environmental Impacts of Karst, Rochester, Minnesota, 5–9 October 2015. NCKRI, Carlsbad, NM, pp. 157–165 published on-line by.
- Shen, H., Xu, Z., Zhang, S., 2016. Review on the simulation of overland flow in hydrological models. *Shuixue Jinzhan/Advances in Water Science* 27:467–475. <https://doi.org/10.14042/j.cnki.32.1309.2016.03.015>.
- Siart, C., Bubenzer, O., Eitel, B., 2009. Combining digital elevation data (SRTM/ASTER), high resolution satellite imagery (Quickbird) and GIS for geomorphological mapping: a multi-component case study on Mediterranean karst in Central Crete. *Geomorphology* 112, 106–121.
- Telbisz, T., Moga, J., 2005. Töbör-morfometriai elemzések a Szilicei-fennsík középső részén (Doline morphological analysis in the central part of the Silická plateau). *Karsztfejlődés* 10, 245–266 (in Hungarian).
- Telbisz, T., Moga, J., Kósik, Sz., 2006. Töbör-morfometriai elemzések a Szilicei-fennsík délnyugati részén (Doline morphological analysis in the south-western part of the Silická plateau). *Karsztfejlődés* 11, 133–152 (in Hungarian).
- Telbisz, T., Látos, T., Deák, M., Székely, B., Koma, Z., Standovár, T., 2016. The advantage of lidar digital terrain models in doline morphometry compared to topographic map based datasets – Aggtelek karst (Hungary) as an example. *Acta Carsologica* 45: 5–18. <https://doi.org/10.3986/ac.v45i1.4138>.
- Tilly, N., Kelterbaum, D., Zeese, R., 2016. Geomorphological mapping with terrestrial laser scanning and uav-based imaging. *Int. Arch. Photogr. Remote Sens. Spat. Inf. Sci.* 41: 591–597. <https://doi.org/10.5194/isprsarchives-XLI-B5-591-2016>.
- Van Den Eeckhaut, N., Kerle, Poesen, J., Hervás, J., 2012. Object-oriented identification of forested landslides with derivatives of single pulse LiDAR data. *Geomorphology* 173–174, 30–42.
- Wall, J., Doctor, D.H., Terziotti, S., 2015. In: Land, L., Doctor, D.H., Stephenson, J.B. (Eds.), *A Semi-Automated Tool for Reducing the Creation of False Closed Depressions From a Filled Lidar-Derived Digital Elevation Model*. NCKRI Symposium 5 Proceedings of the 14th Multidisciplinary Conference on Sinkholes and the Engineering and Environmental Impacts of Karst, Rochester, Minnesota, 5–9 October 2015. NCKRI, Carlsbad, NM, pp. 255–262 published on-line by.
- Wall, J., Bohnenstiehl, D.R., Wegmann, K.W., Levine, N.S., 2017. Morphometric comparisons between automated and manual karst depression inventories in Apalachicola National Forest, Florida, and Mammoth Cave National Park, Kentucky, USA. *Nat. Hazards* 85, 729–749.
- Wechsler, S.P., 2007. Uncertainties associated with digital elevation models for hydrologic applications: a review. *Hydrol. Earth Syst. Sci.* 11, 1481–1500.
- Weishampel, J.F., Hightower, J.N., Chase, A.F., Chase, D.Z., Patrick, R.A., 2011. Detection and morphologic analysis of potential below-canopy cave openings in the karst landscape around the Maya polity of Caracol using airborne LiDAR. *J. Cave Karst Stud.* 73, 187–196.
- Wu, Q., Deng, C., Chen, Z., 2016. Automated delineation of karst sinkholes from LiDAR-derived digital elevation models. *Geomorphology* 266:1–10. <https://doi.org/10.1016/j.geomorph.2016.05.006>.
- Wulder, M., Franklin, S.E., 2012. *Remote Sensing of Forest Environments: Concepts and Case Studies*. Springer Science & Business Media (519 pp).
- Zboray, Z., Bárány Kevei, I., 2004. Domborzatértékelés a Bükk-fennsíkon légifelvételek felhasználásával. (Relief evaluation of Bükk plateau using aerial photographs). *Karsztfejlődés* 9, 207–213 (in Hungarian).